# SI-ATRP grafting of polymers from polydopamine-modified cellulose nanocrystals

Yelin Hou, Zhen Zhang, Simon Harrisson, Gilles Sèbe

# SI-ATRP grafting of polymers from polydopamine-modified cellulose nanocrystals

Yelin Hou[a], Zhen Zhang[*,b], Simon Harrisson[a], Gilles Sèbe[*,a]

[1] Univ. Bordeaux, CNRS, Bordeaux INP, LCPO, UMR 5629, F-33600 Pessac, France

[2] SCNU-TUE Joint Lab of Device Integrated Responsive Materials (DIRM), Institute of Electronic Paper Displays, South China Academy of Advanced Optoelectronics, South China Normal University, Guangzhou 510006, China

*Corresponding authors:

E-mail addresses: gilles.sebe@u-bordeaux.fr (G. Sèbe), zhangzhen@m.scnu.edu.cn (Z. Zhang)

**ABSTRACT**

This work reports on the possibility of using polydopamine (PDA) as a tool to immobilize bromoisobutyryl moieties at the surface of cellulose nanocrystals (CNCs) and initiate Surface Intitiated Atom Transfer Radical Polymerization (SI-ATRP) reactions from these sites. Two different strategies based on i) the stepwise modification of the CNCs with dopamine (DA) and α-bromoisobutyryl bromide (BiBB) (Protocol 1) and ii) the one-step treatment of the CNCs with a mixture of DA and BiBB-modified DA (Protocol 2), were compared. Only the CNC particles treated according to Protocol 1 guaranteed efficient anchoring of the SI-ATRP initiating sites in our experimental conditions (with limited impact on the CNCs crystalline structure), the coated layer being leached out by certain solvents in the case of Protocol 2. The brominated particles displaying the best performances were subsequently tested as potential ATRP macroinitiators, using methyl methacrylate (MMA) and styrene (St) as model monomers.

Polymer-grafted particles were successfully obtained, with a grafting density twice as high for Sty as for MMA, demonstrating the validity of this strategy.

**Keywords**

Cellulose nanocrystals; polydopamine; SI-ATRP; polymethyl methacrylate; polystyrene

## 1. Introduction

With the gradual implementation of the concept of low-carbon environmental protection, the development of environmentally friendly biomass resources has attracted more and more attention (Kobayashi & Nakajima, 2021; Velvizhi et al., 2022). Cellulose nanocrystals (CNCs) are rod-like nanoparticles, typically obtained by acid hydrolysis of cellulosic substrates (pulp, paper or microcrystalline cellulose), which are increasingly considered as building blocks for high-value applications in biotechnology, electronics, optics, energy, packaging or catalysis (Thomas et al., 2018). Their interest lies in particular in their renewable and biocompatible nature, outstanding mechanical properties, high aspect ratio, inclination for chiral nematic ordering, and reactive surface. The efficient use of CNCs however requires a fine control of their dispersive, interfacial and self-assembling properties, which is generally achieved by chemical functionalization of their surface. Polymer grafting by Surface Initiated Atom Transfer Radical Polymerization (SI-ATRP) is particularly attractive in this regard, as it allows nanohybrids with well-controlled surface properties to be obtained after introduction of halogenated sites from which controlled radical polymerization can be initiated (Wohlhauser et al., 2018; Z. Zhang et al., 2021). Until now, the most widely employed method to do so, makes use of an esterification reaction between the surface hydroxyl groups of the CNCs and α-bromoisobutyryl bromide (BiBB). However, direct reaction with the surface cellulose chains can damage the crystalline structure of the particles through surface erosion and/or modification of the cellulose I native allomorph (partial conversion into cellulose II) (Z. Zhang et al., 2021).

To address this issue, an alternative strategy would be to coat the CNCs with a brominated layer made of polydopamine (PDA), which could then be reacted with BiBB, limiting the impact of the treatment on cellulose nanocrystals. Polydopamine (PDA) is a bio-inspired hydrophilic polymer produced by the oxidative polymerization of dopamine (DA) in alkaline conditions, and composed of dihydroxyindole, indolquinone and dopamine units, which are assumed to be covalently linked (Fig. 1). As biocompatible and biodegradable material, PDA has also excellent adhesive properties (Barclay, Hegab, Clarke, & Ginic-Markovic, 2017; Lee, Dellatore, Miller, & Messersmith, 2007; Liu, Ai, & Lu, 2014). Its catechol and amine moieties make it an excellent coating for almost any type of surface including metals, oxides, graphene and synthetic polymers, while at the same time providing reactive sites for further chemical modification (Barclay et al., 2017; Lee et al., 2007; Liu et al., 2014). The mechanism of attachment of PDA on organic and inorganic substrates remains poorly understood, but the presence of both catechol and amine groups seems to be critical; adhesion appears to be the results of a combined variety of noncovalent and covalent connections, within the coating and to the surface, such as π-π stacking, van der Waals forces, hydrophobic associations, hydrogen bonds or electrostatic interactions (Barclay et al., 2017). PDA displays also remarkable properties, which can impart additional functions to the coated material, such as fluorescence, UV-absorption, paramagnetism, radical scavenging activity, electrical conductivity, metal ions chelating activity and redox activity (Barclay et al., 2017; Lee et al., 2007; Liu et al., 2014; Yang et al., 2020). Up to now, the functionalization of CNCs with PDA has been envisaged to graft PEG (Zheng et al., 2021), prepare Janus particles (Sun et al., 2022), crosslink nanofiber mats (Yang et al., 2022) or immobilize cellulase (Qin et al., 2023). Its utilization for the surface immobilization of ATRP initiators has been recently explored with metals (Zhu & Edmondson, 2011), polystyrene (Kohri et al., 2013; Zhu & Edmondson, 2011), graphene oxide (Luo, Zhao, Fei, Liu, & Liu, 2016; Wang et al., 2019), carbon nanotubes (Huang et al., 2020; Song et al.,

2016), $TiO_2$ nanoparticles (Kopeć et al., 2018) or poly(vinylidene fluoride) (Dong et al., 2018). Two types of strategies were then used: in the first one (named Protocol 1 in the current paper), PDA was polymerized in alkaline water on the targeted surface, then the brominated initiator was anchored by reaction between the hydroxyl/amine groups of PDA and BiBB, in dry conditions (Huang et al., 2020; Kopeć et al., 2018; Song et al., 2016; Wang et al., 2019); in the second one (Protocol 2), the BiBB initiator was first reacted *in-situ* with an excess of DA in dry conditions, then the BiBB-modified DA was copolymerized in basic water with the remaining DA (Dong et al., 2018; Kohri et al., 2013; Luo et al., 2016; Zhu & Edmondson, 2011). This second method appears more convenient, as the DA functionalization and oxidative polymerization on CNCs are performed in the same flask, but fewer hydroxyl/amine groups are available after the reaction with BiBB, which may detrimentally impact the binding with the CNCs. To the best of our knowledge, none of these strategies have been applied to cellulose nanocrystals; yet this approach could limit CNCs degradation in ATRP reactions, while at the same time providing additional properties related to the PDA surface layer. There is also a lack of fundamental knowledge concerning the protocols mentioned in the literature, which are mostly implemented as a tool to reach other objectives.

In this work, we investigated the possibility of using PDA chemistry to introduce brominated sites at the CNC surface, and initiate SI-ATRP reactions from these sites. The two functionalization strategies (Protocols 1 & 2) were compared, using different characterization techniques such as X-ray Photoelectron spectroscopy (XPS), X-ray diffraction analysis (XRD), Fourier transform infrared spectroscopy (FT-IR) and solid state $^{13}C$ CP-MAS NMR spectroscopy. The brominated particles displaying the best performances were subsequently tested as potential ATRP macroinitiators, using methyl methacrylate (MMA) and styrene (St) as model monomers. The polymer-grafted CNCs obtained were then examined by FT-IR spectroscopy, $^{13}C$ CP-MAS NMR spectroscopy, thermogravimetric analysis (TGA) and

derivative thermogravimetry (DTG), while the polymerization kinetics were investigated by liquid $^{1}H$ NMR and size-exclusion chromatography (SEC).

## 2. Experimental section

### *2.1. Materials*

Cellulose nanocrystals (CNCs) were provided by the University of Maine (US). They were produced by acid hydrolysis of wood pulp with sulfuric acid, and are composed of rod-shape particles of 110 ± 48 nm in length and 4.8 ± 1.1 nm in thickness, as determined by atomic force microscopy in a previous study (Brand, Pecastaings, & Sèbe, 2017). The particles are decorated with negative sulfate half-ester groups at their surface, resulting from the sulfuric acid treatment. The amount of accessible hydroxyl groups at the surface was estimated at 3.1 ± 0.1 mmol.g$^{-1}$ in the same study. α-bromoisobutyryl bromide (BiBB, >98%), 3-hydroxytyramine hydrochloride (DA, >98%), tris(hydroxymethyl)aminomethane (Tris, >99%), copper(I) bromide (CuBr, >98%), N,N,N′,N″,N″-pentamethyldiethylenetriamine (PMDETA, >99%) were purchased from TCI Europe. Triethylamine (TEA, 99%), methyl methacrylate (MMA, 99%) were purchased from Alfa Aesar 99%. Ethyl α-bromoisobutyrate (EBib, 98%) and styrene (St, 99%) purchased from Sigma Aldrich.

### *2.2. Immobilization of the brominated sites.*

Protocol 1: the CNC-PDA$_{P1}$-Br$_x$ samples (P1 = protocol 1; x = Br atomic % determined by XPS) were prepared by, first coating PDA on the CNCs, then reacting the CNC-PDA material with BIBB, taking inspiration from previous work (Song et al., 2016). In detail, 0.5 g of CNCs were dispersed in 20 mL water through 1 min sonication (Bandelin, MS72 probe). 0.6 g of DA and 70 mL of water were then added to this suspension, which was adjusted to pH = 8.5 with 0.6 g of Tris. The mixture was stirred at room temperature for 24 h. The particles were recovered by centrifugation, washed three times with water/centrifugation cycles, then freeze-dried. The esterification reaction was performed in DMF, under nitrogen, in the presence of equal volumes

of TEA and BiBB. Before reaction, the CNC-PDA material was dispersed in 30 mL DMF (through 1 min sonication), while BiBB (1, 2, or 4 mL) was solubilized in 10 mL DMF. After solubilization of TEA in the CNC-PDA suspension, an ice bath was added and the BiBB solution was introduced dropwise. After 30 min, the ice bath was removed, and the reaction was conducted for 24 h. The particles were recovered by centrifugation, then washed/centrifugated with i) ethanol, ii) water (until the supernatant was colorless), and finally freeze-dried. To further probe the stability of the grafting towards the solvents used in the ATRP experiments, additional washing/centrifugation steps were later performed with i) DMF and ii) THF, followed by a dialysis in water for 3 days using a 3.5 kDa regenerated cellulose ester dialysis membrane.

Protocol 2: the CNC-$PDA_{P2}$-$Br_x$ samples (P2 = protocol 2; x = Br atomic % determined by XPS) were prepared by co-polymerizing a mixture of DA and BiBB-modified DA on the CNCs surface, taking inspiration from previous work (Kohri et al., 2013). The BiBB-modified DA was first prepared by reacting DA with BiBB in DMF, under nitrogen, with equal volume amounts of TEA as catalyst (0.9 molar equivalents). 0.6 g of DA were solubilized in 5 mL DMF with TEA, then various amounts of BiBB (1, 2, or 4 mL) were added and stirred for 3h at room temperature. The reaction with the CNCs was performed in the same flask, in a second step. The CNCs suspension (0.5 g of CNCs in 20 mL water) was added to the previous mixture with 70 mL of additional water, and the pH was adjusted to 8.5 with Tris. The direct reaction between the CNCs and unreacted BiBB cannot be totally excluded at this stage, but the hydrolysis of BiBB should be largely favored. The oxidative polymerization was allowed to proceed for 24 h at room temperature, then the particles were centrifugated/washed with ethanol/water then DMF/THF as described before (Protocol 1).

### *2.3. SI-ATRP grafting of PMMA and PS.*

The CNC-$PDA_{P1}$-$Br_{1.44}$ sample was used as macroinitiator to initiate the SI-ATRP

polymerizations. Reactions were conducted in DMF, with methyl methacrylate (MMA) and styrene (St) as model monomers, Cu(I)Br as catalyst, pentamethyldiethylenetriamine (PMDETA) as ligand and ethyl α-bromoisobutyrate (EiBB) as sacrificial initiator. Reactions with MMA were performed at 60°C, with a molar ratio of [MMA]:[EBib]:[CuBr]:[PMDETA]=300:1:1:1. Reactions with St were performed at 100°C, with a molar ratio of [St]:[EBib]:[CuBr]:[PMDETA]=500:1:1:1. In detail, 50 mg of CNC-$PDA_{P1}$-$Br_{1.44}$ particles were dispersed in 11.6 mL DMF through sonication. 150 mmol MMA (15 mL) or 250 mmol St (28 mL),0.5 mmol EBiB (70 μL) and 0.5 mmol PMDETA (105 μL) were added to the mixture. The dispersion was bubbled with argon for 30 min. And then 0.5 mmol CuBr (70 mg, weighted in a glove box), was added to the mixture. After degassing by three freeze-pump-thaw cycles under argon, the reaction flask was immersed in an oil bath at the required temperature. Different operations were performed at designed polymerization time (20 min, 40 min, 60 min, 90 min, 120 min & 180 min): i) 40 μL of the reaction medium was withdrew and added in 460 μL $CDCl_3$ for $^1$H NMR characterization (evaluation of the monomer conversion); ii) 1mL of the reaction medium was withdrawn, centrifugated, passed through a neutral $Al_2O_3$ column with THF as solvent (to remove copper and retain any dispersed CNC particles), then poured into methanol to precipitate the free polymer for SEC analysis. At the end of the SI-ATRP reaction (90 min for MMA, 7h for St), the whole reaction mixture was centrifuged several times with i) THF and ii) ethanol (until the supernatant was colorless), and the sedimented particles were dried under vacuum at 50 °C before FT-IR and CP-MAS $^{13}$C NMR characterization. The supernatant from the final centrifugation was collected and characterized by $^1$H NMR to confirm that no free macromolecules were left.

### 2.4. *Fourier-Transform Infrared spectroscopy (FT-IR).*

FT-IR spectra were recorded in the 4000-450 $cm^{-1}$ range, using a Bruker Vertex 70 spectrometer, at a resolution of 4 $cm^{-1}$ (64 scans). Sampling was performed with the potassium bromide method. For ease of comparison, the spectra were normalized to the C-O stretching vibration of cellulose at 1060 $cm^{-1}$.

### 2.5. *X-ray photoelectron spectrometry (XPS)*

A ThermoFisher Scientific K-ALPHA spectrometer was used for XPS surface analysis, with a monochromatized Al-Kα source (hν = 1486.6 eV) and a 400 µm X-Ray spot size. Powders were pressed onto indium foils. The full survey spectra (0-1100 eV) were obtained with a constant pass energy of 200 eV.

### 2.6. *Nuclear Magnetic Resonance spectroscopy (NMR)*

CP-MAS $^{13}C$ NMR analysis of the CNC-PDA, CNC-$PDA_{p1}$-$Br_{1.44}$ and PMMA@CNC-$PDA_{p1}$-$Br_{1.44}$ samples was performed by the CESAMO platform of the Institute of Molecular Sciences (ISM, Talence, France). Measurements were done at 25 °C, with a Bruker Avance II 400 spectrometer operating at a frequency of 100.63 MHz (conventional CP-MAS method). The zirconium oxide rotors containing the samples were spun at 8 kHz, while the 90° pulse, contact time, and repetition time were set at 2.8 µs, 2.0 ms, and 4 s, respectively. The PS@CNC-$PDA_{p1}$-$Br_{1.44}$ sample was analysed by the Institut Européen de Chimie et Biologie (IECB, Pessac, France), using a Bruker Avance III spectrometer (Wissembourg, France) operating at 125MHz, with a 4 mm double resonance HX-CPMAS probe. The sample packed in a 4 mm zirconium rotor (Cortecnet, Voisin Le Bretonneux) was spun at 11kHz, with the following acquisition parameters: 5 s recycling delay, 2k scans, 1 ms or 4 ms for contact time (temperature during acquisition ≈ 35°C). $^{13}C$ chemical shifts are reported relative to the carbonyl of glycine (external reference) at 173.6 ppm, and spectra are phased and baseline-corrected.

The monomer conversion during SI-ATRP reaction was evaluated by liquid $^{1}H$ Nuclear

Magnetic Resonance (NMR), using a Bruker Avance 400 ($^1$H at 400 MHz) spectrometer, with deuterated chloroform ($CDCl_3$) as solvent.

### *2.7. X-Ray Diffraction spectroscopy (XRD)*

XRD analyses were performed by the Centre de Recherche Paul Pascal (CRPP, Pessac, France). Measurements were conducted on a Rigaku Nanoviewer (XRF microsource generator, MicroMax 007HF), with a rotating anode coupled to a confocal Max-Flux® Osmic mirror (Applied Rigaku Technologies, Austin, USA) producing beam with a wavelength of 1,5418A° or an energy of 8KeV. The sample was put in a glass capillary and exposed to the X-Ray beam for 90min. Data were collected on a MAR345 image plate detector (MARResearch, Norderstedt, Germany) placed at a distance of 129 mm, providing access to 2Theta angle in the 5-40° range. Images were collected and spectra integrated with the FIT2D software (ERSF; http://www.esrf.eu/).

The crystallinity Index (CrI) was estimated from the diffractograms by the Segal method (Segal, Creely, Martin, & Conrad, 1959):

$$CrI = \frac{I_{22.6°} - I_{18.3°}}{I_{22.6°}} \qquad (2\text{-}1)$$

where $I_{22.6°}$ represents the intensity of the (200) crystallographic plane of cellulose $I_\beta$ and $I_{18.3°}$ the intensity of the amorphous contribution. The average dimensions of the elementary crystallites perpendicular to the (200) plan ($L_{200}$) were estimated from Scherrer's equation:

$$L_{200} = \frac{0.9\lambda}{\beta cos\theta} \qquad (2\text{-}2)$$

where θ is the diffraction angle, λ is the wavelength of the X-ray radiation, and β is the full width at half height of the diffraction peak.

### *2.8. Size-Exclusion Chromatography (SEC)*

The molecular weight of the free polymers produced during SI-ATRP was measured by Size-exclusion chromatography (SEC), with tetrahydrofuran (THF) as the eluent. Samples were analyzed after vacuum drying and dispersion in THF (5g/L), using an Ultimate 3000 system

(Thermoscientific) equipped with a diode array detector, a multi-angles light scattering detector and differential refractive index detector (Wyatt technology). Polymers were separated on three G2000, G3000 and G4000 TOSOH HXL gel columns (300 x 7.8 mm) (exclusion limits from 200 Da to 400 000 Da) with a flowrate of 1 mL/min at 40°C. The elution times were converted to molar mass using a calibration curve based on PS or PMMA standards.

### *2.9. Thermogravimetric analysis (TGA)*

TGA experiments were conducted on a TGA Q500 instrument. Samples (8-10 mg) were heated up to 600°C, at a rate of 10 °C.min$^{-1}$ and under nitrogen atmosphere (flow rate: 40 mL.min$^{-1}$ for balance, 60 for furnace). The weight loss was recorded as a function of temperature, and the temperature of maximum degradation was obtained from the maximum of the derivative curve. The grafting density after ATRP reaction was estimated from the thermograms of the PMMA@CNC-PDA$_{p1}$-Br$_{1.44}$ and PS@CNC-PDA$_{p1}$-Br$_{1.44}$ samples, by calculating the ratio of second weight loss due to the polymer (between 330 and 450 °C) relative to the first weight loss due to CNC-PDA degradation (between 120 and 330 °C). Ratios of 1.3 and 1.1 were measured with PMMA and PS, respectively. These ratio were later converted in mmol of grafted polymer *per* gram of CNC-PDA material using the $M_n$'s of free PMMA (22650 g.mmol$^{-1}$) and PS (5928 g.mmol$^{-1}$) determined by SEC: grafting density with PMMA = 1.3/22.650 = 0.057 mmol/g; grafting density with PS = 1.1/5.928 = 0.186 mmol.g$^{-1}$. To improve the accuracy in the case of PMMA, the grafting density was re-calculated taking into account the 10 % weight loss that PMMA undergoes in the 150-330 temperature range: corrected second weight loss = (1.3x100)/90 = 1.44 g; corrected first weight loss = 1-(1.44-1.3) = 0.86 g; corrected grafting density = (1.44/0.86)/22.650 = 0.074 mmol.g$^{-1}$.

### *2.10. Atomic Force Microscopy (AFM)*

The morphology of the polymer-grafted samples was assessed by AFM, in tapping mode. Samples were dispersed in water (0.2 g.L$^{-1}$) by sonicating the mixture for 2 min (Bandelin,

MS72 probe). One droplet of the dispersion was then deposited on a freshly cleaved mica surface priorly treated by a 10 mM $MgCl_2$ aqueous solution. After overnight air-drying, the samples were observed with a Dimension Fastscan AFM (Bruker) microscope in tapping mode (at 22°C), using a FastScan-A probe. The nominal spring constant was set to 18 $N.m^{-1}$ and the resonance frequency to 1.400 Hz. Height and phase images were obtained using a scan rate of 3.8 Hz, and analyzed by the NanoScope Analysis software.

## 3. Results and Discussion

### *3.1. Immobilization of the brominated sites through PDA coating*

Two different strategies were investigated to introduce the brominated initiating sites at the surface of the CNCs (Fig. 1). With Protocol 1, the CNCs were reacted with DA and BiBB in a stepwise manner, while with Protocol 2, the CNC surface was modified in one step, by co-polymerizing a mixture of DA and BiBB-modified DA. After reaction, samples were extensively washed with ethanol and water, to remove any unreacted product and traces of triethylamine (Zeng et al., 2017; Zhu & Edmondson, 2011). The two protocols were compared in term of Br grafting achieved when an equal amount of BiBB was used in each process, the Br content being measured by XPS.

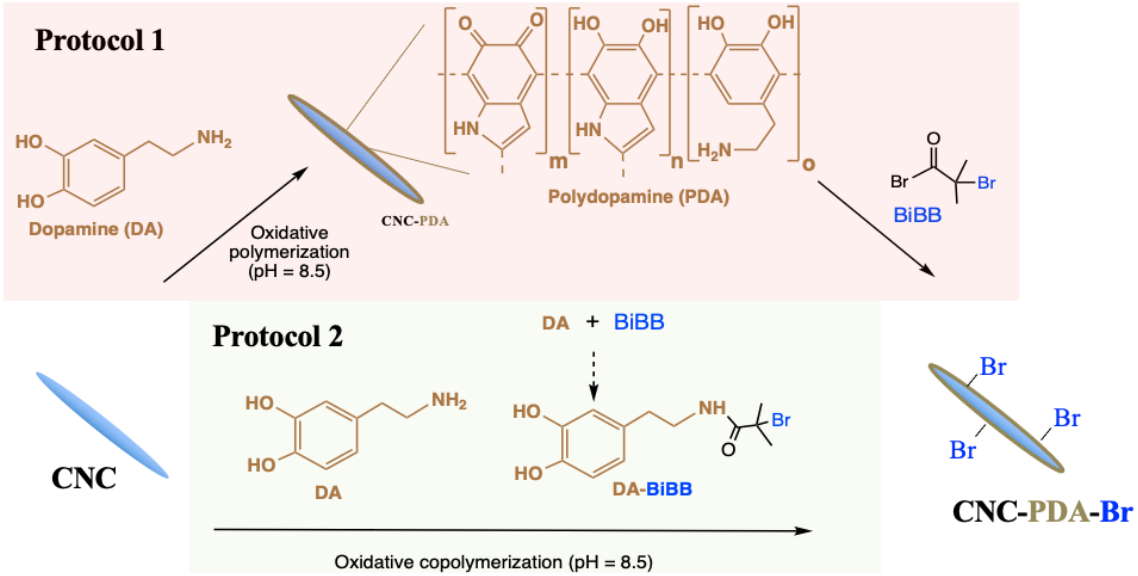


**Fig. 1.** Immobilization of the brominated initiating sites by polydopamine chemistry; two different protocols were investigated (Protocol 1 & 2).

The reaction conditions and bromine content obtained after reaction with increasing amounts BiBB are summarized in Table 1. The crystallinity index (CrI) and average dimensions of the elementary crystallites perpendicular to the (200) plan ($L_{200}$), measured for the particles treated with Protocol 1, are also reported. The corresponding XPS survey spectra with the relative elemental composition at the nanoparticles surface are presented in Fig. S1 & S2 and Tables S1 & S2 in Supporting Information. With protocol 1, the amount of Br sites immobilized at the CNCs surface could be easily controlled by adjusting the BiBB volume, the reaction with the PDA-modified CNCs being increasingly favored when more BiBB was used; but quite a large excess of BiBB was required to achieve high bromine content. Higher grafting levels could be obtained with Protocol 2, using lower amounts of BiBB, but this process required an optimization of the BiBB amount (at about 2 mL), as the efficiency decreased when the BiBB was too high (*i.e.* 4 mL). With this second protocol, the Br immobilization is achieved by first partially functionalizing some of the DA molecules with BiBB, then co-reacting this DA-BiBB

precursor with pristine DA by reductive oxidation, in the presence of the CNCs. Since hydroxyl/amine groups are required for both the coupling between DA-BiBB and DA, and the binding with the CNC surface, a decreased efficiency is expected when the DA-BiBB monomer is excessively substituted by the bromoisobutyryl moieties (*i.e.* when 4 mL of BiBB is used in our case). The concentration of unmodified DA remaining in the medium may be also too low when an excessive concentration of BiBB is used.

**Table 1.** Br content measured by XPS after modification with Protocol 1 or 2 and extensive washing with ethanol and water.

| Reaction conditions | | | | Protocol 1 | | | | Protocol 2 | |
|---|---|---|---|---|---|---|---|---|---|
| CNCs (3.1 mmol OH/g)* | DA | BiBB Volume (mL) | BiBB Molar Content (mmol) | Samples | Br content (Atom. %) | CrI (%) | $L_{200}$ (nm) | Samples | Br content (Atom. %) |
| 0.5 g (1.55 mmol OH) | 0.6 g (3.18 mmol) | 1 | 8.1 | CNC-$PDA_{P1}$-$Br_{0.22}$ | 0.22 | 85 | 4.3 | CNC-$PDA_{P2}$-$Br_{1.44}$ | 1.44 |
| | | 2 | 16.2 | CNC-$PDA_{P1}$-$Br_{1.05}$ | 1.05 | 71 | 4.0 | CNC-$PDA_{P2}$-$Br_{1.98}$ | 1.98 |
| | | 4 | 32.4 | CNC-$PDA_{P1}$-$Br_{1.44}$ | 1.44 | 70 | 4.0 | CNC-$PDA_{P2}$-$Br_{0.43}$ | 0.43 |

CNCs: CrI = 86 %; $L_{200}$ = 4.4 nm; *Brand, Pecastaings, & Sèbe, 2017

The grafting was further confirmed through the observation of the characteristic vibrations of the bromoisobutyryl moieties in the infrared spectra (Fig. 2). The emerging bands observed in the spectra of Fig. 2a and 2b indicate that the bromoisobutyryl moieties were grafted at both the phenolic ($\nu_{C=O}$ at 1760 $cm^{-1}$) and amine sites ($\nu_{C=O}$ at 1650-1630 $cm^{-1}$, $\delta_{N-H}$ at 1510 $cm^{-1}$) of PDA, regardless of the protocol. To make sure that the grafting was resistant to the solvents used in the subsequent ATRP treatment, the brominated samples were further washed successively by DMF and THF (under sonication), and analyzed again by FT-IR spectroscopy (Fig. S3 in Supporting Information). No modification of the infrared pattern was noted with Protocol 1 (Fig. S3a), but the bromoisobutyryl signals of the protocol 2 samples disappeared (Fig. S3b), indicating that the PDA coating was not strongly bonded in that case. Less

hydroxyl/amine groups are available for the bonding with the CNCs surface with Protocol 2, as part of these sites are already substituted by BiBB before the oxidative reaction. It is therefore likely that the amount of free hydroxyl/amine groups is not sufficient to guarantee an efficient anchoring at the CNCs surface, the PDA layer being solubilized by DMF and/or THF. In view of these results, only the particles modified with Protocol 1 were used in subsequent experiments.

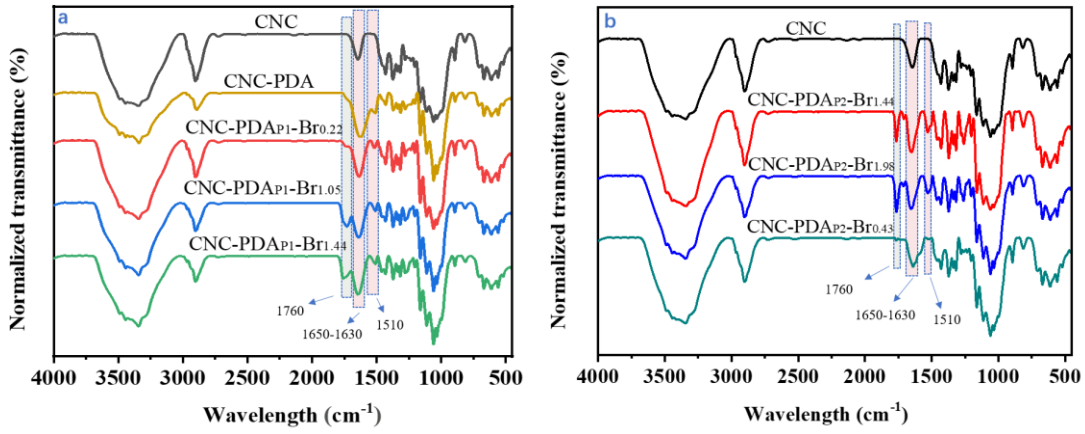


**Fig. 2.** FT-IR spectra of the brominated CNCs obtained from Protocol 1 (a) and Protocol 2 (b), after washing with ethanol and water.

Further confirmation of the bromoisobutyryl grafting was provided by solid state $^{13}C$ CP-MAS NMR analysis, as shown in Fig. 3. To help in the assignment, the spectrum of the CNCs modified with pure PDA (CNC-PDA) is also reported. The signals of cellulose are observed at 110 ppm ($C_1$), 95 ppm ($C_4$ crystalline), 89 ppm ($C_4$ amorphous), 76-80 ppm ($C_2$, $C_3$, $C_5$), 69 ppm ($C_6$ crystalline), 67 ppm ($C_6$ amorphous) (Atalla, Gast, Sindorf, Bartuska, & Maciel, 1980), while the PDA pattern can be seen in the 115-150 ppm (arene carbons) and 30-60 ppm (cyclized aliphatic carbons) regions (Dreyer, Miller, Freeman, Paul, & Bielawski, 2012). After reaction with BiBB, the bromoisobutyryl signals emerge at 178 ppm (C=O), 60 ppm (C-Br) and 37 ppm ($CH_3$).

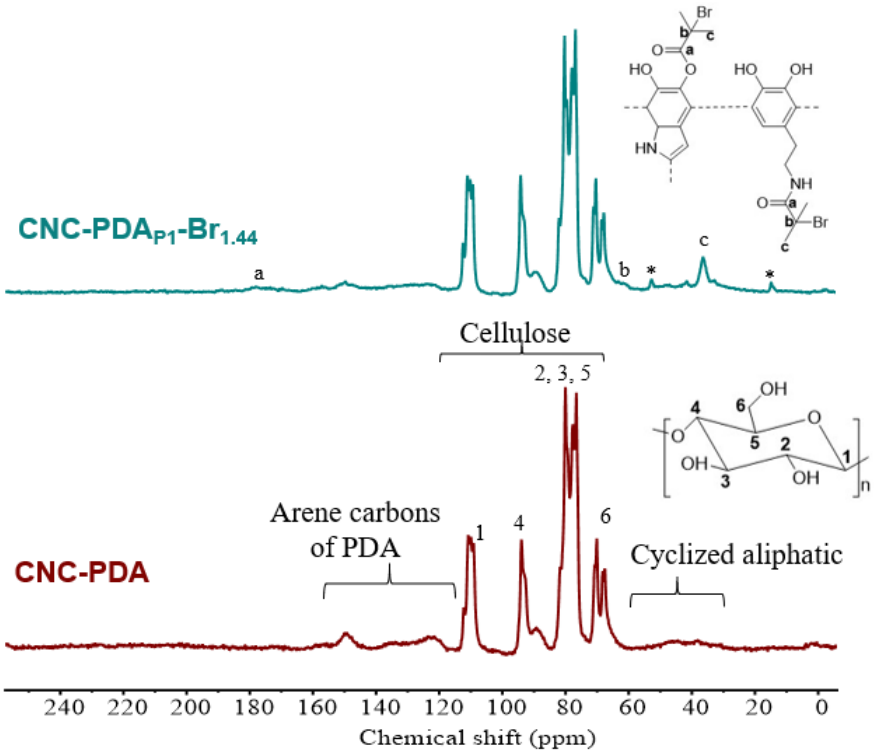


**Fig. 3.** $^{13}$C CP-MAS NMR spectrum of the CNC-PDA$_{P1}$-Br$_{1.44}$ sample obtained from Protocol 1 (the peaks identified by an asterisk* are assigned to traces of triethylamine). The spectrum of the CNCs modified with pure PDA (CNC-PDA) is also reported.

The impact of the Protocol 1 treatment on the CNCs crystalline structure was assessed by X-ray diffraction analysis (XRD) (Fig. 4), through the calculation of i) the crystallinity index (CrI) measured by the Seagal method (Segal et al., 1959), and ii) the average dimension of the elementary crystallites perpendicular to the (200) plan ($L_{200}$) estimated from Scherrer's equation (Sebe, Ham-Pichavant, Ibarboure, Koffi, & Tingaut, 2012). In Fig. 4, the characteristic diffraction peaks of the cellulose I pattern can be seen at $2\theta = 15$, 17, 20, 22.3 and 34.5°, corresponding to the $(1\bar{1}0)$, (110), (012), (200) and (004) diffraction planes, respectively, while pure PDA is amorphous. The peak at $2\theta = 12°$ was assigned to traces of cellulose II. A slight decrease in CrI and $L_{200}$ was noted after the successive reactions with DA and BiBB, but the

particles remained highly crystalline, indicating that the Protocol 1 treatment did not significantly impact the nanoparticles' structure. The slight decrease in crystallinity can be partly assigned to the amorphous fraction brought by the PDA layer. When the CNC surface was directly esterified with the classical method (without PDA), a significant decrease in crystallinity was noted when 2 and 4 mL of BiBB were used (Fig. S4), confirming the interest of Protocol 1 to preserve the nanoparticles structure.

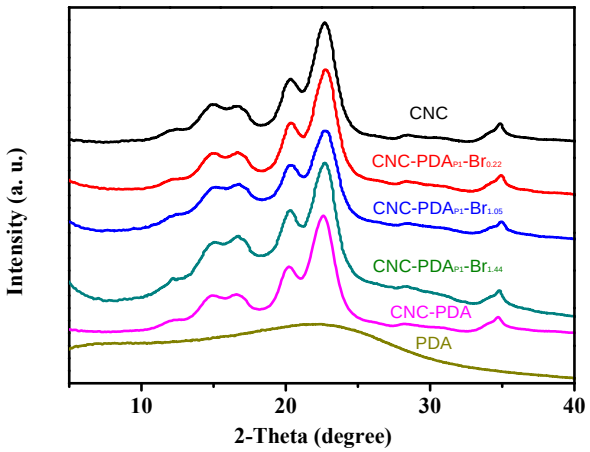


**Fig. 4**. XRD spectra of the brominated CNCs obtained with Protocol 1. The spectra of pristine CNCs and CNCs modified with pure PDA (CNC-PDA) are also reported.

### 3.2. *SI-ATRP grafting of PMMA and PS*

ATRP experiments were performed with methyl methacrylate (MMA) and styrene (Sty) as model monomers, in a standard set of conditions inspired from the literature (Chun-xiang, Huai-yu, Ming-hua, Shi-yu, & Jia-jun, 2009; Z. Zhang, Wang, Tam, & Sebe, 2019). The CNC-PDA$_{P1}$-Br$_{1.44}$ sample, with the highest bromine content, was used as initiating substrate. Reactions were conducted in DMF, with MMA and Sty as model monomers, Cu(I)Br as catalyst, pentamethyldiethylenetriamine (PMDETA) as ligand and ethyl α-bromoisobutyrate (EiBB) as sacrificial initiator (Fig. 5).

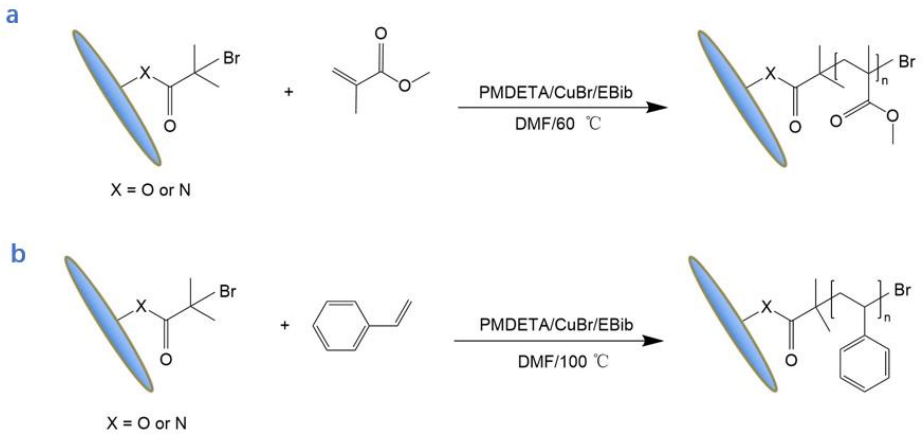


**Fig. 5.** SI-ATRP grafting of MMA (a) and Sty (b) from the CNC-PDA$_{P1}$-Br$_{1.44}$ sample.

The successful grafting of PMMA and PS was first confirmed by FT-IR spectroscopy (Fig. 6a and 6c). The infrared vibrations of grafted PMMA are observed at 2996/2949 cm$^{-1}$ ($\nu_{C-H}$) and 1735cm$^{-1}$ ($\nu_{C=O}$), while those of PS emerge at 3058/3026 cm$^{-1}$ ($\nu_{CH\ aromatic}$), 1602/1492/1452 cm$^{-1}$ ($\nu_{C=C}$), 698/757 cm$^{-1}$ ($\gamma_{C-H}$). Further confirmation of the grafting was provided by the solid state $^{13}$C CP-MAS NMR spectra, through the observation of the characteristic signals of PMMA at 183 ppm (c), 61 ppm (a), 57 ppm (d), 50 ppm (b) and 22 ppm (e) (Fig. 6b), and of PS at 150 ppm (a'), 132 ppm (b'), 46-54 ppm (c'), 44 ppm (d') (Fig.6d). The AFM analysis of the polymer-grafted samples indicated that the rod-like morphology of the nanocrystals was

retained (Fig. S5), but an accurate estimation of the dimensions could not be inferred from the pictures as the particles significantly aggregated during deposition on the mica surface.

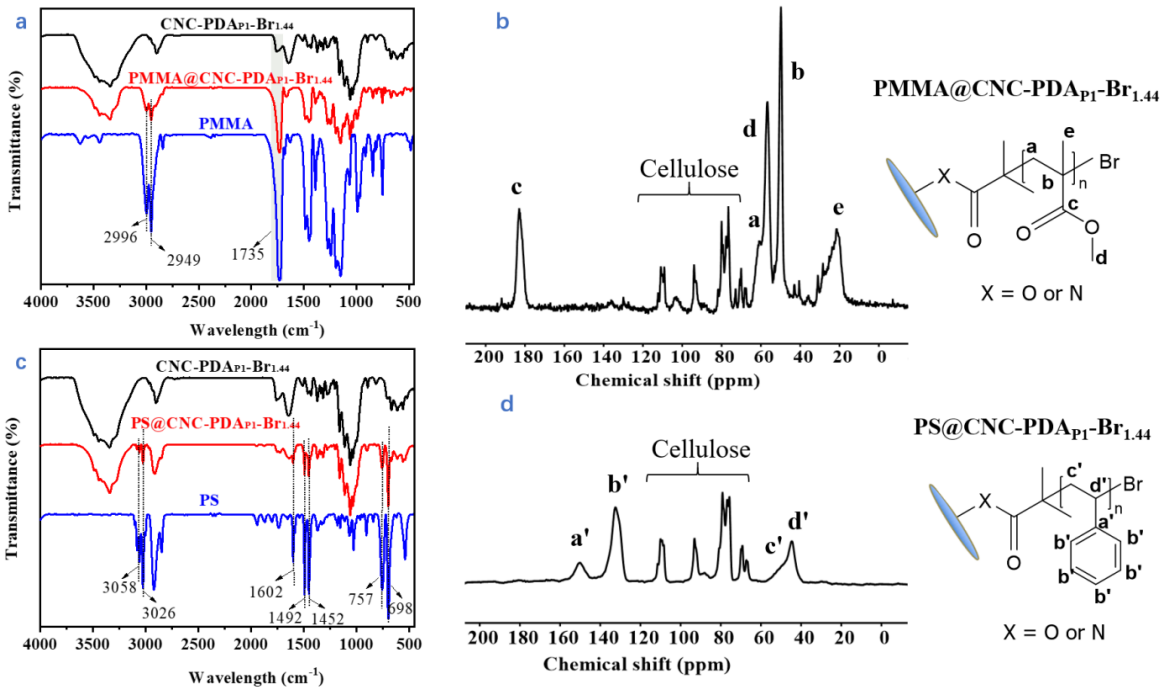


**Fig. 6.** FT-IR (a, c) and $^{13}C$ CP-MAS NMR (b, d) spectra of the CNC-PDA$_{P1}$-Br$_{1.44}$ particles before and after SI-ATRP grafting of MMA or Sty. The FT-IR spectra of the free polymers are also reported.

The kinetics of the reactions were investigated by analyzing the free polymer produced by the sacrificial initiator, assuming that the molecular weights of the grafted and free polymers were similar (Fig. 7). With both monomers, the number-average molecular weight ($M_n$) of the PMMA and PS increased linearly with the monomer conversion and the dispersity (Đ) remained relatively low (less than 1.3 for PMMA and 1.4 for PS). In the case of MMA, the $M_n$ determined by SEC was twice as high as expected (Fig. 7a), while the first-order kinetic plot of $\ln([M_0]/[M_t])$ shows a positive intercept (Fig. 7b). Taken together, these elements suggest that a significant amount of initial termination occurred with PMMA, leading to loss of approximately 50% of

the EiBB in the very early stages of the reaction, as the concentration of $Cu(II)Br_2$ built up to sufficient levels to control the reaction. These results are consistent with previous observations of low initiator efficiency of EiBB in ATRP polymerization of MMA (T. Zhang, Gieseler, & Jordan, 2016). After the first 20 minutes, $\ln([M_0]/[M_t])$ increased linearly with time, indicating a first order reaction with a near constant concentration of radicals, as expected in ATRP reactions. In the case of Sty, good agreement between expected and $M_n$ determined by SEC was observed (Fig. 7c), while the first-order kinetic plot showed some deviations from linearity, indicating a low level of ongoing termination reactions and gradual decrease in the radical concentration (Fig. 7d). The reactions proceeded at substantially different rates, reflecting the different reactivities of the chain ends towards activation and deactivation (Li, Wang, Li, & Zhu, 2011): after 90 min of reaction, the MMA polymerization had reached *c.* 40% conversion and an $M_n$ of 22650 $g.mol^{-1}$, while that of Sty attained only *c.* 12% conversion and 5928 $g.mol^{-1}$ after 7 hours.

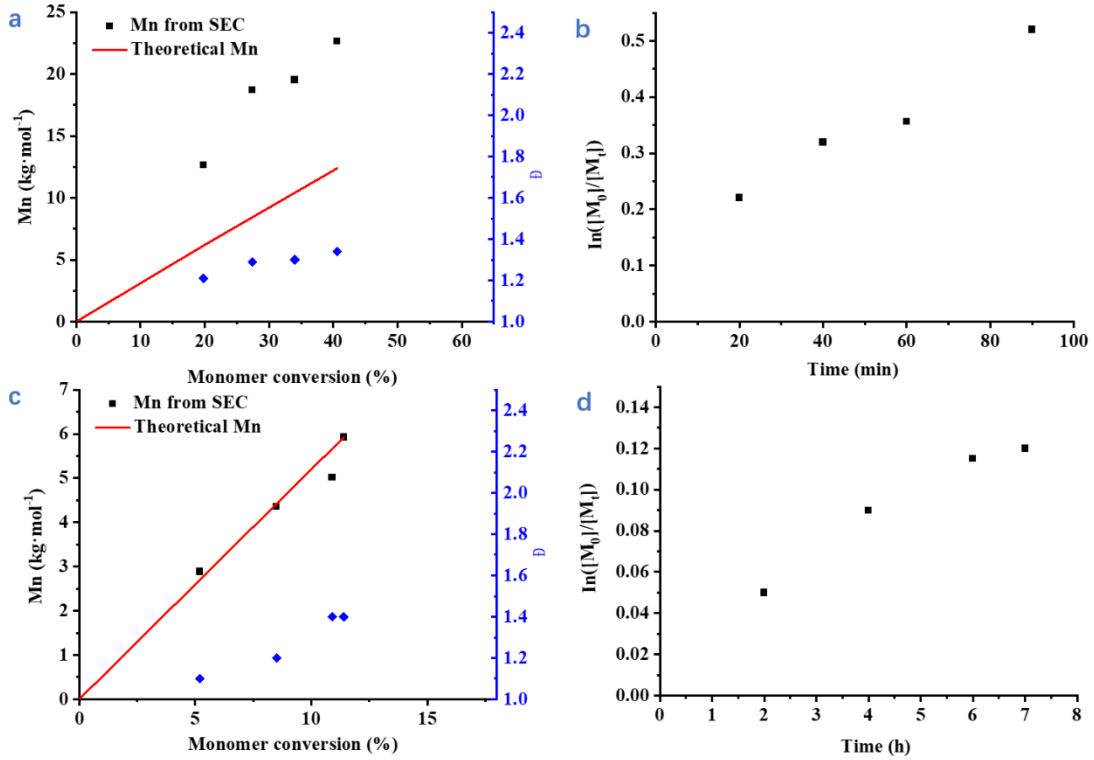


**Fig. 7.** Kinetics of the ATRP reactions with MMA (a, b) and Sty (c, d): (a), (c) $M_n$ and dispersity (Đ) *vs.* monomer conversion; (b), (d) ln([$M_0$]/[$M_t$]) *vs.* time.

The thermal stability of the polymer-grafted particles was investigated by thermogravimetric analysis (TGA), the thermograms at each step of the treatments being gathered in Fig. 8, with the data of the free polymers. The corresponding DTG curves are presented in Fig. S6.

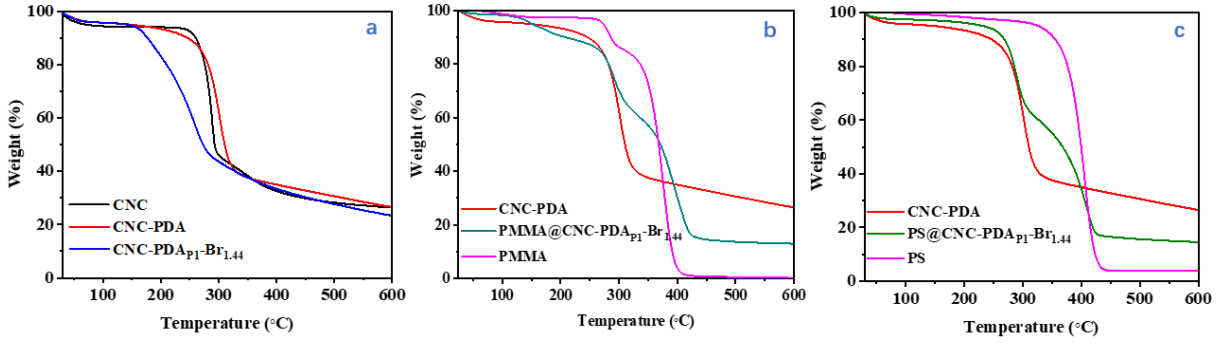


**Fig. 8.** TGA thermograms of the different samples before (a) and after the ATRP reaction with

412 MMA (b) and Sty (c). The data obtained with the free polymers and CNC-PDA particles are
413 also reported in b and c.
414
415 The thermogram of unmodified particles in Fig. 8a is characteristic of CNCs produced by
416 sulfuric acid hydrolysis, with first, evaporation of water at 25-100 °C, then decomposition of
417 cellulose with a temperature of maximum rate of degradation ($T_{max}$) of 287 °C. After the DA
418 treatment (CNC-PDA), a slight increase in $T_{max}$ is noted (at 300 °C), indicating that the PDA
419 layer retarded cellulose degradation to some extent. Further modification with BiBB (CNC-
420 $PDA_{p1}$-$Br_{1.44}$) led to a significant decrease in the thermal stability of the cellulosic material
421 (degradation started at 150 °C), which may be related to the strong hydrobromic acid released
422 upon heating, due to the labile bromine (Wohlhauser, Rader, & Weder, 2022). After the PPMA
423 or PS grafting on the other hand (PMMA@CNC-$PDA_{p1}$-$Br_{1.44}$ and PS@CNC-$PDA_{p1}$-$Br_{1.44}$,
424 respectively in Fig. 8b and 8c), the thermal stability is recovered, the cellulose chains being
425 now protected by the grafted polymers, while the brominated moieties are no longer in close
426 proximity to the nanocrystals (see Fig. 5). A two-step profile is now observed, corresponding
427 to, first the degradation of cellulose coated with PDA (at $T_{max}$ = 289 °C for PMMA@CNC-
428 $PDA_{p1}$-$Br_{1.44}$ and 290 °C for PS@CNC-$PDA_{p1}$-$Br_{1.44}$), followed by the degradation of grafted
429 PMMA (at $T_{max}$ = 387-404 °C) or PS (at $T_{max}$ = 407 °C). The ratio of the second weight loss
430 (polymer) relative to the first weight loss (CNC-PDA material) was then used to estimate the
431 grafting density, expressed in mmol of grafted polymer *per* gram of CNC-PDA material, based
432 on the $M_n$'s measured by SEC (see experimental section). The method is expected to be quite
433 accurate for the PS-grafted particles, as the degradation of PS and CNC-PDA material do not
434 overlap. An underestimation of the grafting density is however expected in the case of
435 PMMA@CNC-$PDA_{p1}$-$Br_{1.44}$, as 10 % of the polymer degrades in the same temperature range
436 as the CNC-PDA material (see thermogram of free PMMA in Fig. 8b). This weight loss,

observed under nitrogen, has been assigned in the literature to the decomposition of the PMMA end-chains (at about 290°C), while random scission (main degradation) takes place between 300 and 400 °C (Hirata, Kashiwagi, & Brown, 1985; Meneghetti & Qutubuddin, 2006). Hence, to improve the accuracy of the grafting density estimation with PMMA, we re-calculated it taking into account this 10 % weight loss, which was added to the polymer loss and subtracted from the CNC-PDA loss (see experimental section). A grafting density of 0.074 mmol.g$^{-1}$ was found for PMMA, which was roughly half that observed for PS (0.186 mmol.g$^{-1}$). The reduced grafting density of PMMA may be a result of the high level of termination observed in the early stages of the PMMA polymerization, which led to loss of approximately 50% of the EiBB, and may be assumed to have consumed a similar fraction of grafted initiator sites.

## 4. Conclusions

We have developed a convenient method to immobilize SI-ATRP initiating sites at the surface of cellulose nanocrystals (CNCs), using polydopamine (PDA) as an intermediate layer. The stepwise modification of the CNCs with dopamine (DA) and α-bromoisobutyryl bromide (BiBB) led to the strong anchoring of brominated sites, with limited impact on the CNCs structure. Weaker anchoring was observed when the CNCs were treated in one step, with a mixture of DA and BiBB-modified DA, presumably because this second approach produced fewer anchoring sites for the bonding with the CNCs. The coating produced in this case resisted solvent washing by ethanol and water, but not by DMF and THF. The best-performing brominated particles were subsequently tested as potential ATRP macroinitiators, using methyl methacrylate (MMA) and styrene (St) as model monomers. First order reactions with a near constant concentration of radicals were inferred from the analysis of free polymers produced by the sacrificial initiator, as expected in ATRP reactions. Reaction with Sty proceeded at substantially lower rate than with MMA, although the grafting density at the CNCs surface was

twice as high. These results illustrate the potential of PDA chemistry as a tool for tailoring the surface chemistry of CNCs by SI-ATRP, while limiting deterioration of the nanoparticles structure. The method may also provide functionality related to the specific properties of PDA (UV-absorption, paramagnetism, radical scavenging activity, electrical conductivity...), which will be investigated in future work.

## Supplementary material

Additional information includes i) the XPS survey spectra with elemental composition of the brominated CNCs, ii) the FT-IR spectra after DMF/THF washing of the brominated CNCs, iii) the XRD spectra of the brominated CNCs obtained by direct esterification with BiBB, iv) the AFM topography images of the samples after SI-ATRP grafting and v) the DTG curves of the samples after SI-ATRP grafting.

## Acknowledgements

The authors gratefully acknowledge financial support from China Scholarship Council (CSC). We also thank the Centre de Recherche Paul Pascal (CRPP, Pessac, France) for the XRD analyses, the Structural Physico-Chemistry platform of the Institut Européen de Chimie et Biologie (IECB, Pessac, France) and CESAMO platform of the Institut des Sciences Moléculaires (ISM, Talence, France) for the NMR experiments, and the PLACAMAT platform of the Institut de Chimie de la matière Condensée (ICMCB, Pessac, France) for the XPS.

## References


Atalla, R. H., Gast, J. C., Sindorf, D. W., Bartuska, V. J., & Maciel, G. E. (1980). Carbon-13 NMR spectra of cellulose polymorphs. *Journal of the American Chemical Society,* 102(9), 3249-3251. https://doi.org/10.1021/ja00529a063

Barclay, T. G., Hegab, H. M., Clarke, S. R., & Ginic-Markovic, M. (2017). Versatile Surface Modification Using Polydopamine and Related Polycatecholamines: Chemistry, Structure, and Applications. *Advanced Materials Interfaces,* 4(19). https://doi.org/10.1002/admi.201601192

Brand, J., Pecastaings, G., & Sèbe, G. (2017). A versatile method for the surface tailoring of cellulose nanocrystal building blocks by acylation with functional vinyl esters. *Carbohydrate Polymers,* 169, 189-197. https://doi.org/10.1016/j.carbpol.2017.03.077

Chun-xiang, L., Huai-yu, Z., Ming-hua, L., Shi-yu, F., & Jia-jun, Z. (2009). Preparation of cellulose graft poly(methyl methacrylate) copolymers by atom transfer radical polymerization in an ionic liquid. *Carbohydrate Polymers,* 78(3), 432-438. https://doi.org/10.1016/j.carbpol.2009.04.032

Dong, L., Liu, X., Xiong, Z., Sheng, D., Lin, C., Zhou, Y., & Yang, Y. (2018). Preparation of UV-blocking poly(vinylidene fluoride) films through SI-AGET ATRP using a colorless polydopamine initiator layer. *Industrial & Engineering Chemistry Research,* 57(38), 12662-12669. https://doi.org/10.1021/acs.iecr.8b02373

Dreyer, D. R., Miller, D. J., Freeman, B. D., Paul, D. R., & Bielawski, C. W. (2012). Elucidating the structure of poly(dopamine). *Langmuir,* 28(15), 6428-6435. https://doi.org/10.1021/la204831b

Hirata, T., Kashiwagi, T., & Brown, J. E. (1985). Thermal and oxidative degradation of poly(methyl methacrylate): weight loss. *Macromolecules,* 18(7), 1410-1418. https://doi.org/10.1021/ma00149a010

Huang, H., Liu, M., Xu, D., Mao, L., Huang, Q., Deng, F., . . . Wei, Y. (2020). Facile fabrication of glycosylated and PEGylated carbon nanotubes through the combination of mussel inspired chemistry and surface-initiated ATRP. *Materials Science and Engineering C,* 106. https://doi.org/10.1016/j.msec.2019.110157

Kobayashi, T., & Nakajima, L. (2021). Sustainable development goals for advanced materials provided by industrial wastes and biomass sources. *Current Opinion in Green and Sustainable Chemistry,* 28, 100439. https://doi.org/10.1016/j.cogsc.2020.100439

Kohri, M., Kohma, H., Shinoda, Y., Yamauchi, M., Yagai, S., Kojima, T., Kishikawa, K. (2013). A colorless functional polydopamine thin layer as a basis for polymer capsules. *Polymer Chemistry,* 4(9), 2696-2702. https://doi.org/10.1039/c3py00181d

Kopeć, M., Spanjers, J., Scavo, E., Ernens, D., Duvigneau, J., & Julius Vancso, G. (2018). Surface-initiated ATRP from polydopamine-modified $TiO_2$ nanoparticles. *European Polymer Journal,* 106, 291-296. https://doi.org/10.1016/j.eurpolymj.2018.07.033

Lee, H., Dellatore, S. M., Miller, W. M., & Messersmith, P. B. (2007). Mussel-inspired surface chemistry for multifunctional coatings. *Science,* 318(5849), 426-430. https://doi.org/10.1126/science.1147241

Li, X., Wang, W. J., Li, B. G., & Zhu, S. (2011). Kinetics and modeling of solution ARGET ATRP of styrene, butyl acrylate, and methyl methacrylate. *Macromolecular Reaction Engineering,* 5(9-10), 467-478. https://doi.org/10.1002/mren.201100024

Liu, Y., Ai, K., & Lu, L. (2014). Polydopamine and its derivative materials: synthesis and promising applications in energy, environmental, and biomedical fields. *Chemical Reviews,* 114(9), 5057-5115. https://doi.org/10.1021/cr400407a

Luo, J., Zhao, F., Fei, X., Liu, X., & Liu, J. (2016). Mussel inspired preparation of polymer grafted graphene as a bridge between covalent and noncovalent methods. *Chemical Engineering Journal,* 293, 171-181. https://doi.org/10.1016/j.cej.2016.02.057

Meneghetti, P., & Qutubuddin, S. (2006). Synthesis, thermal properties and applications of polymer-clay nanocomposites. *Thermochimica Acta,* 442(1-2), 74-77. https://doi.org/10.1016/j.tca.2006.01.017

Qin, T., Liu, L., Cao, H., Lu, B., Nie, S., Cheng, Z., Zhang, X., Liu, H., & An, X. (2023). Polydopamine modified cellulose nanocrystals (CNC) for efficient cellulase immobilization towards advanced bamboo fiber flexibility and tissue softness. *International Journal of Biological Macromolecules,* 253, 126734. https://doi.org/10.1016/j.ijbiomac.2023.126734

Sebe, G., Ham-Pichavant, F., Ibarboure, E., Koffi, A. L., & Tingaut, P. (2012). Supramolecular structure characterization of cellulose II nanowhiskers produced by acid hydrolysis of cellulose I substrates. *Biomacromolecules,* 13(2), 570-578. https://doi.org/10.1021/bm201777j

Segal, L., Creely, J. J., Martin, A. E., & Conrad, C. M. (1959). An empirical method for estimating the degree of crystallinity of native cellulose using the X-ray diffractometer. *Textile Research Journal,* 29(10), 786-794. https://doi.org/10.1177/004051755902901003

Song, Y., Ye, G., Lu, Y., Chen, J., Wang, J., & Matyjaszewski, K. (2016). Surface-initiated ARGET ATRP of poly(glycidyl methacrylate) from carbon nanotubes via bioinspired catechol chemistry for efficient adsorption of uranium ions. *ACS Macro Letters,* 5(3), 382-386. https://doi.org/10.1021/acsmacrolett.6b00099

Sun, Q., Xiao, L., Nie, Y., Wang, W., Bai, L., Chen, H., Yang, L., Yang, H., & Wei, D. (2022). Fabrication of Janus-type nanocomposites from cellulose nanocrystals for self-healing hydrogels' flexible sensors. *Colloids and Surfaces B: Biointerfaces,* 216, 112554. https://doi.org/10.1016/j.colsurfb.2022.112554

Thomas, B., Raj, M. C., Joy, J., Moores, A., Drisko, G. L., & Sanchez, C. (2018). Nanocellulose,

562 a versatile green platform: from biosources to materials and their applications. *Chemical*
563 *Reviews,* 118(24), 11575-11625. https://doi.org/10.1021/acs.chemrev.7b00627
564 Velvizhi, G., Goswami, C., Shetti, N. P., Ahmad, E., Kishore Pant, K., & Aminabhavi, T. M.
565 (2022). Valorisation of lignocellulosic biomass to value-added products: Paving the
566 pathway towards low-carbon footprint. *Fuel,* 313, 122678.
567 https://doi.org/10.1016/j.fuel.2021.122678
568 Wang, S., Meng, H., Li, Y., Sun, D., Zhan, Y., Ge, X., & Chen, L. (2019). Polymer brushes
569 grafted from graphene via bioinspired polydopamine chemistry and activators
570 regenerated by electron transfer atom transfer radical polymerization. *Journal of*
571 *Polymer Science, Part A: Polymer Chemistry,* 57(6), 689-698.
572 https://doi.org/10.1002/pola.29310
573 Wohlhauser, S., Delepierre, G., Labet, M., Morandi, G., Thielemans, W., Weder, C., & Zoppe,
574 J. O. (2018). Grafting polymers from cellulose nanocrystals: synthesis, properties, and
575 applications. *Macromolecules,* 51(16), 6157-6189.
576 https://doi.org/10.1021/acs.macromol.8b00733
577 Wohlhauser, S., Rader, C., & Weder, C. (2022). Facile method to determine the molecular
578 weight of polymer grafts grown from cellulose nanocrystals. *Biomacromolecules,* 23(3),
579 699-707. https://doi.org/10.1021/acs.biomac.1c01050
580 Yang, L., Liu, X., Zhang, X., Chen, T., Ye, Z., & Rahaman, M. S. (2022). High performance
581 nanocomposite nanofiltration membranes with polydopamine-modified cellulose
582 nanocrystals for efficient dye/salt separation. *Desalination,* 521.
583 https://doi.org/10.1016/j.desal.2021.115385
584 Yang, P., Zhang, S., Chen, X., Liu, X., Wang, Z., & Li, Y. (2020). Recent developments in
585 polydopamine fluorescent nanomaterials. *Materials Horizons,* 7(3), 746-761.
586 https://doi.org/10.1039/c9mh01197h

587 Zeng, Z., Wen, M., Ye, G., Huo, X., Wu, F., Wang, Z., Yan, J., Matyjaszewski, K., Lu, Y., &
588 Chen, J. (2017). Controlled architecture of hybrid polymer nanocapsules with tunable
589 morphologies by manipulating surface-initiated ARGET ATRP from hydrothermally
590 modified polydopamine. *Chemistry of Materials,* 29(23), 10212-10219.
591 https://doi.org/10.1021/acs.chemmater.7b04319
592 Zhang, T., Gieseler, D., & Jordan, R. (2016). Lights on! A significant photoenhancement effect
593 on ATRP by ambient laboratory light. *Polymer Chemistry,* 7(4), 775-779.
594 https://doi.org/10.1039/C5PY01858G
595 Zhang, Z., Sèbe, G., Hou, Y., Wang, J., Huang, J., & Zhou, G. (2021). Grafting polymers from
596 cellulose nanocrystals via surface-initiated atom transfer radical polymerization.
597 *Journal of Applied Polymer Science,* 138(48). https://doi.org/10.1002/app.51458
598 Zhang, Z., Wang, X., Tam, K. C., & Sebe, G. (2019). A comparative study on grafting polymers
599 from cellulose nanocrystals via surface-initiated atom transfer radical polymerization
600 (ATRP) and activator re-generated by electron transfer ATRP. *Carbohydrate Polymers,*
601 205, 322-329. https://doi.org/10.1016/j.carbpol.2018.10.050
602 Zheng, T., Clemons, C. M., & Pilla, S. (2021). Grafting PEG on cellulose nanocrystals via
603 polydopamine chemistry and the effects of PEG graft length on the mechanical
604 performance of composite film. *Carbohydrate Polymers,* 271, 118405.
605 https://doi.org/10.1016/j.carbpol.2021.118405
606 Zhu, B., & Edmondson, S. (2011). Polydopamine-melanin initiators for surface-initiated ATRP.
607 *Polymer,* 52(10), 2141-2149. https://doi.org/10.1016/j.polymer.2011.03.027
608
609
610
611